

Article

# High-Efficiency Visible Light Responsive Sulfide $\text{KSb}_5\text{S}_8$ Photocatalyst with a Layered Crystal Structure

Yuanyuan Li <sup>1,2,\*</sup> , Meijun Wu <sup>1</sup>, Qiang Wang <sup>1,2</sup>, Kun Wang <sup>3</sup>, He Zhang <sup>3</sup>, Xuejun Quan <sup>3</sup>, Bin Zhang <sup>4,\*</sup> and Dingfeng Yang <sup>3,\*</sup>

<sup>1</sup> Department of Biological and Chemical Engineering, Chongqing University of Education, Chongqing 400067, China; meijunwu123@163.com (M.W.); gogo1443@sina.com (Q.W.)

<sup>2</sup> Cooperative Innovation Center of Lipid Resources and Children's Daily Chemicals, Chongqing University of Education, Chongqing 400067, China

<sup>3</sup> College of Chemistry and Chemical Engineering, Chongqing University of Technology, 69 Hongguang Rd., Lijiatuo, Banan District, Chongqing 400054, China; wk1434182820@163.com (K.W.); zh944756928@163.com (H.Z.); hengjunq@cqut.edu.cn (X.Q.)

<sup>4</sup> Analytical and Testing Center of Chongqing University, Chongqing 401331, China

\* Correspondence: liyy@cque.edu.cn (Y.L.); welon5337@126.com (B.Z.); yangxunscience@cqut.edu.cn (D.Y.); Tel.: +86-1590-230-5519 (Y.L.)

Received: 28 April 2019; Accepted: 11 June 2019; Published: 13 June 2019



**Abstract:** The development of efficient photocatalysts for degrading environmental pollutants in wastewater has drawn considerable attention due to their great potential in industrial applications. Herein, we used a solvothermal method to prepare  $\text{KSb}_5\text{S}_8$  with a layered crystal structure. The crystal structure of the as-synthesized samples was characterized by powder X-ray diffraction and transmission electron microscope imaging. Our UV-vis diffuse reflectance spectroscopy results indicated that  $\text{KSb}_5\text{S}_8$  could absorb visible light, and its optical band gap was 1.62 eV. The photocatalytic activity of  $\text{KSb}_5\text{S}_8$  was evaluated in the degradation of methyl orange. A degradation of 73% within 180 min was achieved under visible light irradiation, which was considerably higher than that of commercial P25 and g- $\text{C}_3\text{N}_4$ . Theoretical calculations demonstrated that  $\text{KSb}_5\text{S}_8$  was an indirect band gap semiconductor. The estimated effective mass of holes ( $m_h^*$ ) was approximately two times greater than that of electrons ( $m_e^*$ ). The large ratio of  $m_h^*/m_e^*$  might promote separation of photo-induced carriers during the photocatalytic process. On the basis of the layered crystal structure and large  $m_h^*/m_e^*$  value,  $\text{KSb}_5\text{S}_8$  was a high-performance photocatalyst capable of harvesting visible light. This study provides valuable insight that will aid the design of improved sulfide photocatalytic materials with layered crystal structures.

**Keywords:** layered crystal structure; visible light; photocatalyst  $\text{KSb}_5\text{S}_8$ ; effective mass

## 1. Introduction

Environmental pollution is becoming more serious owing to continuing population growth. Semiconductor photocatalysts can be applied in environmental purification and play an important role in the processing of wastewater [1,2]. Many photocatalysts have been reported to date.  $\text{TiO}_2$  is a particularly effective and commonly used photocatalyst, which has been intensively investigated due to its abundance, intrinsic physical properties, high chemical stability, and potential for applications [3,4]. However, due to the intrinsic large band gap (3.2 eV),  $\text{TiO}_2$  is only responsive to ultraviolet radiation, which accounts for 4% of the solar spectrum [5]. Furthermore, recombination of photo-induced electrons and holes severely reduces its photocatalytic efficiency. Therefore, practical applications of  $\text{TiO}_2$  have been limited to date [6]. Strategies such as ion doping, heterojunction construction,

and noble metal loading have been developed to enhance the absorption of visible light and accelerate the separation of photo-induced electrons and holes [7–10]. However, the overall efficiencies achieved to date remain low. The development of novel photocatalysts with high performance in the visible light region has drawn considerable research interest.

Compared to metal oxide photocatalysts, metal sulfides have narrow band gaps and more dispersive band edges with a smaller effective mass of photo-induced carriers, which might satisfy the needs for high performance visible light driven photocatalysts [11,12]. In addition, materials with layered crystal structures have a short distance for photo-induced carriers to migrate and diffuse to the surface reactive site, which might reduce the possibility of electron–hole recombination and contribute to higher quantum yields [13,14]. Many layered compounds, such as WS<sub>2</sub> [15], SnS<sub>2</sub> [16], MnPSe<sub>3</sub> [17], and Bi<sub>2</sub>WO<sub>6</sub> [18], have been predicted to be excellent photocatalysts. Furthermore, compounds with layered crystal structures, such as g-C<sub>3</sub>N<sub>4</sub> and BiOCl, have shown to have good photocatalytic performance [19,20]. Herein, we propose an engineering process based on the crystallographic structural design and electronic structure analysis to identify layered sulfide compounds with excellent photocatalytic performance.

KSb<sub>5</sub>S<sub>8</sub> is a typical ternary sulfide semiconductor, which has a natural layered structure of the space group *P*<sub>n</sub> [21,22]. In this research, for the first time, we applied a simple solvothermal method to prepare KSb<sub>5</sub>S<sub>8</sub> and evaluated its photocatalytic activity in the degradation of a methyl orange (MO) dye solution under visible light irradiation. In these experiments, 73% of the MO solution was degraded within 180 min under visible light irradiation. Theoretical calculations revealed that the high degradation efficiency might originate from the intrinsic small carrier effective mass and the large ratio of  $m_h^*/m_e^*$ , which contributed to the separation of photo-induced carriers during the photocatalytic process. On the basis of our analyses of the crystal and electronic structure, we propose ternary sulfide KSb<sub>5</sub>S<sub>8</sub> as an efficient photocatalyst for applications under visible light irradiation.

## 2. Results and Discussion

We prepared the KSb<sub>5</sub>S<sub>8</sub> sample using a simple solvothermal method, and the phase was characterized by powder X-ray diffraction (XRD). In Figure 1, Rietveld fitting indicated that all peaks of the KSb<sub>5</sub>S<sub>8</sub> were indexed to the monoclinic structure of space group *P*<sub>n</sub> (NO. 7) and no secondary phases were detected, indicating the purity of the as-synthesized KSb<sub>5</sub>S<sub>8</sub>. The refined cell parameters of KSb<sub>5</sub>S<sub>8</sub> were  $a = 8.1582 \text{ \AA}$ ,  $b = 19.5585 \text{ \AA}$ ,  $c = 9.1084 \text{ \AA}$ ,  $\beta = 91.8371^\circ$ , and  $V = 1452.6072 \text{ \AA}^3$ , respectively, which were in good agreement with previous reports [23]. As shown in Figure 2, the crystal structure of KSb<sub>5</sub>S<sub>8</sub> can be described as a layered structure with infinite undulating slabs of [Sb<sub>5</sub>S<sub>8</sub>]<sup>−</sup>, where the K<sup>+</sup> ions are located in the interlayer space to balance the charge. The Sb atoms were surrounded by S atoms to form SbS<sub>3</sub>, SbS<sub>4</sub>, and SbS<sub>5</sub> groups in the layer of [Sb<sub>5</sub>S<sub>8</sub>]<sup>−</sup>, with covalent Sb–S bond length ranging from 2.438 Å to 2.807 Å. Weaker ionic K–S (3.242 Å–3.760 Å) bonds connected the interlayer to build the crystal structure.

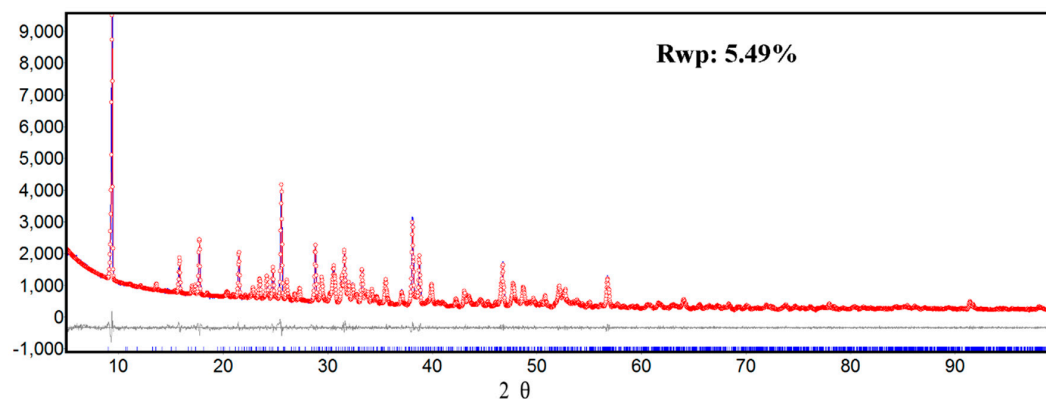
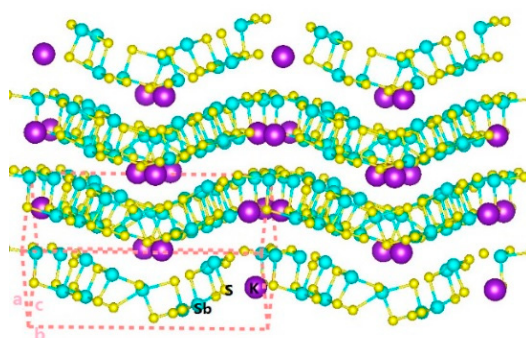
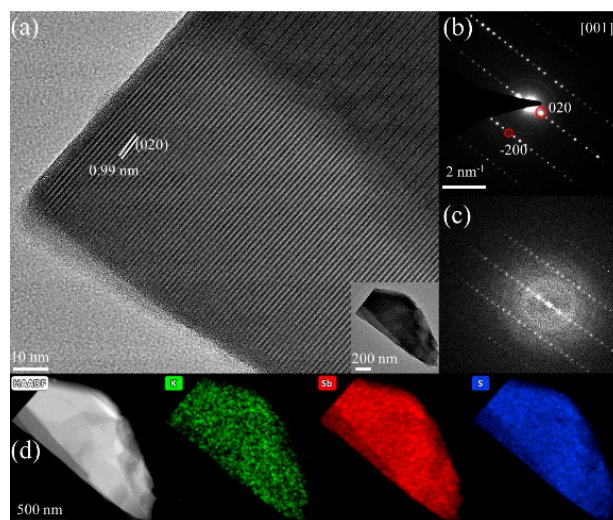


Figure 1. Powder X-ray diffraction patterns of as-synthesized KSb<sub>5</sub>S<sub>8</sub> samples via Rietveld refinement.



**Figure 2.** The schematic photograph of  $\text{KSb}_5\text{S}_8$ . Purple, cyan, and yellow balls indicate K, Sb, and S atoms, respectively.

We studied the structure further investigated by transmission electron microscope (TEM) imaging. Figure 3a shows a high magnification TEM image (with a flake morphology inset) composed of clear and well-defined lattice, indicating the good crystallinity of the  $\text{KSb}_5\text{S}_8$ . The inter-planar spacing was  $\sim 0.99$  nm, corresponding to the (020) planes of  $\text{KSb}_5\text{S}_8$ . Figure 3b,c shows the corresponding selected area electron diffraction (SAED) and fast Fourier transformation (FFT) patterns of the grain in Figure 3a, respectively. The patterns were well indexed to the {001} orientation. Here, the bright spots in the SAED pattern indicated good crystallization and the single crystalline nature of the flake (inset in Figure 3a). The energy dispersion spectrometry (EDS) maps (Figure 3d) confirmed that the constituent elements (i.e., K, Sb, and S) were distributed homogeneously throughout the sample.



**Figure 3.** (a) TEM image of  $\text{KSb}_5\text{S}_8$ . (b,c) Experimental selected area electron diffraction (SAED) and fast Fourier transformation (FFT) patterns along the [001] zone axis. (d) Energy dispersion spectrometry (EDS) elemental mappings of  $\text{KSb}_5\text{S}_8$ .

The optical properties of the as-synthesized  $\text{KSb}_5\text{S}_8$  sample were characterized by UV-vis diffuse reflectance spectroscopy (UV-vis DRS). As shown in Figure 4, the calculated band gap was 1.62 eV, which was consistent with the dark red color of the crystal, demonstrating that  $\text{KSb}_5\text{S}_8$  might be a visible light harvesting photocatalytic material.

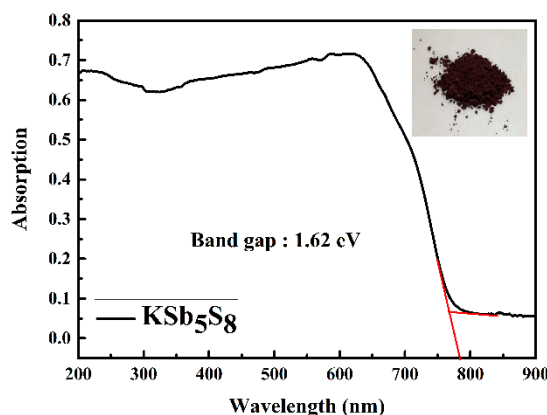


Figure 4. UV-visible absorption spectra of  $\text{KSb}_5\text{S}_8$  sample (inset: Dark red).

The photocatalytic activity of  $\text{KSb}_5\text{S}_8$  was first evaluated through the degradation of the MO solution under visible light irradiation ( $\lambda \geq 420$  nm). Commercial P25 and layered state-of-the-art photocatalyst  $\text{g-C}_3\text{N}_4$  were also included for reference. Prior to the light irradiation, the adsorption–desorption balance was achieved between the photocatalyst and the MO solution under intense stirring and dark condition after 60 min. In Figure 5a, the photocatalytic reaction of MO in the absence of a photocatalyst was negligible under visible light. However,  $\text{KSb}_5\text{S}_8$  exhibited an excellent photocatalytic performance, and more than 73% of MO was degraded within 180 min, whereas the proportion degraded by P25 and  $\text{g-C}_3\text{N}_4$  was only approximately 8% and 15%, respectively. The UV-vis absorption spectra (Figure S1) and the photograph of the dye solution (Figure S2) also indicated that the original color of the solution gradually decolorized over  $\text{KSb}_5\text{S}_8$ .

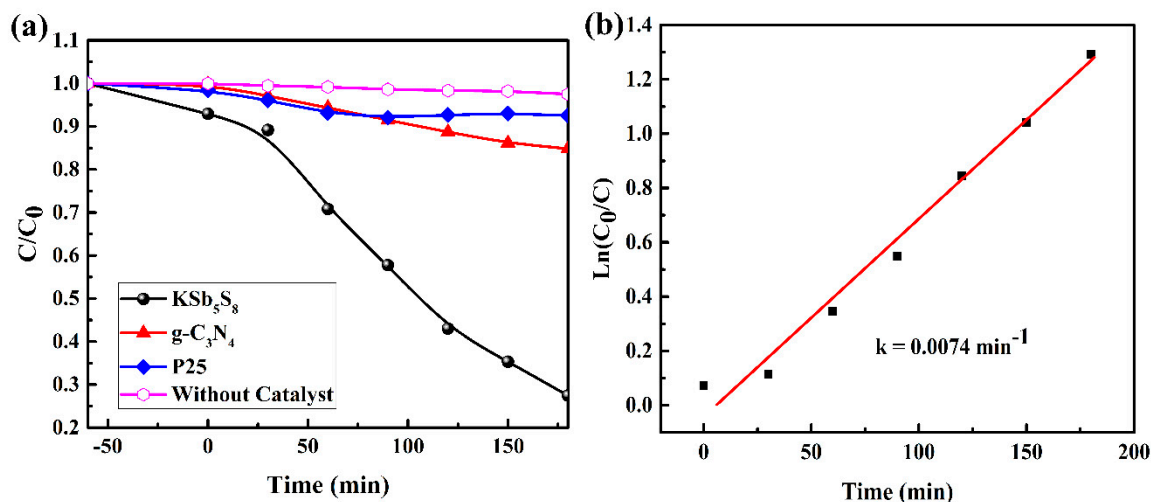


Figure 5. (a) Photocatalytic degradation curves of methyl orange (MO) over P25,  $\text{g-C}_3\text{N}_4$ , and  $\text{KSb}_5\text{S}_8$  under visible light irradiation. (b) Corresponding linear fitting curve of  $\ln C_0/C$  as a function of time for  $\text{KSb}_5\text{S}_8$ .

To quantitatively study the reaction kinetics, the photocatalytic processes can be understood by the Langmuir–Hinshelwood kinetics model, assuming that the reaction conformed to a pseudo first order model [24].

$$\ln \frac{C_t}{C_0} = -kt$$

where  $C_t$  ( $\text{mol}\cdot\text{L}^{-1}$ ),  $C_0$  ( $\text{mol}\cdot\text{L}^{-1}$ ), and  $k$  ( $\text{min}^{-1}$ ) represent the initial concentration of the MO solution after the absorption equilibrium, the instantaneous concentration of MO at time  $t$  and the apparent

reaction rate constant, respectively. The corresponding apparent photocatalytic reaction rate of  $\text{KSb}_5\text{S}_8$  from the experimental data was fitted as  $0.0074 \text{ min}^{-1}$  (Figure 5b).

The stability of the photocatalyst was another critical issue for its practical application. Sulfide photocatalysts in particular tend to undergo photocorrosion, which decreases their photocatalytic activity. To evaluate the stability of as-synthesized  $\text{KSb}_5\text{S}_8$  particles, we examined the cycling performance. The results are shown in Figure S3. The photocatalytic activity remained greater than 65% after two cycles. However, the activity decreased markedly to approximately 25% after three cycles. We detected precipitation of sulfur in the XRD patterns of  $\text{KSb}_5\text{S}_8$  after three cycles of MO degradation (Figure S4), which indicated that photocorrosion occurred during the photocatalytic process.

To further understand the mechanism of the photocatalytic degradation, a schematic picture of the redox potential of  $\text{KSb}_5\text{S}_8$  with the generation of reactive species for the photodegradation of the MO solution was proposed. Generally, the band edge potentials of a valence band (VB) and a conduction band (CB), designated as  $E_{\text{VB}}$  and  $E_{\text{CB}}$ , can be calculated according to the following empirical equations [25]:

$$E_{\text{VB}} = \chi - E_e + 0.5E_g \quad (1)$$

$$E_{\text{CB}} = E_{\text{VB}} - E_g \quad (2)$$

where  $\chi$  is the absolute electronegativity of a semiconductor, which is described as the geometric average of the absolute electronegativity of the individual atom,  $E_e$  is the energy of free electrons on the hydrogen scale (4.5 eV), and  $E_g$  is the optical band gap. The calculated values of  $E_{\text{VB}}$  and  $E_{\text{CB}}$  for  $\text{KSb}_5\text{S}_8$  were 1.60 eV and 0.01 eV, respectively. On the basis of the alignment of the above energy levels, we confirmed the possibility of the oxidation mechanism proposed in Figure 6.

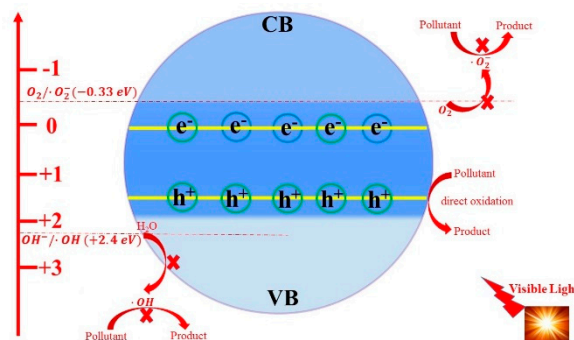


**Figure 6.** Possible mechanism of photocatalytic degradation of MO solution over  $\text{KSb}_5\text{S}_8$  under visible light.

Generally, active species, including super radical anion ( $\cdot\text{O}_2^-$ ), free hydroxyl radical ( $\cdot\text{OH}$ ), and photo-induced holes ( $h^+$ ), are related to the photocatalytic degradation reaction [26]. Photo-induced electrons ( $e^-$ ) and holes ( $h^+$ ) can transfer to the surface of crystals and then react with molecular oxygen ( $\text{O}_2$ ) and  $\text{H}_2\text{O}$  molecules to produce superoxide radical anion ( $\cdot\text{O}_2^-$ ) and free hydroxyl radical ( $\cdot\text{OH}$ ), respectively. These free radicals work as strong oxidizing agents for degrading organic molecules. We note that the redox pairs  $\cdot\text{OH}/\text{OH}^-$  (2.38 eV vs. NHE) are more positive than the  $E_{\text{VB}}$ , and the redox pairs  $\text{O}_2/\text{O}_2^-$  ( $-0.33 \text{ eV}$  vs. NHE) are more negative than  $E_{\text{CB}}$  [27]. Therefore, thermodynamically, holes cannot oxidize the  $\text{OH}^-$  to produce  $\cdot\text{OH}$ ; meanwhile,  $\cdot\text{O}_2^-$  cannot be yielded by the reduction of electrons. We speculate that the degradation reaction might originate from direct transfer of  $h^+$  to oxidize the MO dye molecules. We also conducted the trapping experiments of photocatalytic active species during the degradation of the MO solution. As presented in Figure S5, we observed that  $h^+$  was the dominant active species in the photocatalytic degradation, whereas  $\cdot\text{OH}$  and  $\cdot\text{O}_2^-$  had little effect. These results were in good accordance with the theoretical analysis above.

To gain better insight into the cause of these excellent photocatalytic properties of  $\text{KSb}_5\text{S}_8$ , we performed theoretical calculations based on density functional theory (DFT). We focused solely on

the electronic states near the valence band maximum (VBM) and the conduction band minimum (CBM) where the photo-induced electrons and holes were generated. In Figure 7a, the band structures of  $\text{KSb}_5\text{S}_8$  feature an indirect band gap with the VBM at D point and the CBM at B point. The calculated band gap value (1.6 eV) was very close to the value obtained from the UV-vis absorption spectra. Next, we considered the effective masses at VBM and CBM. Generally, the effective mass can be extracted from the second derivate of the energy level of band edges through the following equation [28]:

$$m^* = \mp \hbar^2 (\partial^2 E_n(k) / \partial k^2)^{-1}, \quad (3)$$

where  $E_n(k)$  is the band energy for n-th band level in k reciprocal lattice space. A small effective mass corresponds to a higher carrier mobility, and a larger value ratio of  $m_h^*/m_e^*$  means a big difference of the migration rate of electrons and holes. Thus, a lower recombination probability occurs. Herein, the value of  $m_h^*/m_e^*$  for  $\text{KSb}_5\text{S}_8$  was approximately 2, which was greater than that of the state-of-the-art photocatalyst  $\text{BiVO}_4$  [29] ( $m_h^*/m_e^* \sim 1$ ). These results indicated that  $\text{KSb}_5\text{S}_8$  had excellent band edge characteristics for photo-induced carrier separation. As shown in Figure 7b, we calculated the total and partial density of states near the band edge. The VBM mainly originated from the S-p states, whereas the CBM mostly consisted of S-p and Sb-p states. The partial charge density offered a visual picture to analyze the band edge of an orbital composition. We observed that the photo-induced carriers were mostly surrounded by the S and Sb atoms (Figure S6).

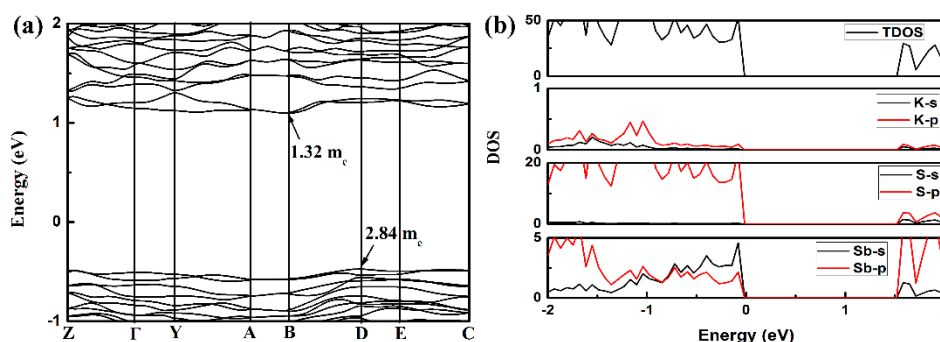


**Figure 7.** (a) Band structure of  $\text{KSb}_5\text{S}_8$  with effective mass at valence band maximum (VBM) and conduction band minimum (CBM). (b) Total and partial density of states of  $\text{KSb}_5\text{S}_8$ .

We attributed the excellent potential of  $\text{KSb}_5\text{S}_8$  as a photocatalyst to two aspects. First,  $\text{KSb}_5\text{S}_8$  featured a layered crystal structure where electrons and holes can move more easily to the edge of the surface. Second, the electronic structure analysis suggested that the photo-induced carriers were highly delocalized in the slab  $[\text{Sb}_5\text{S}_8]^-$  and the ratio of  $m_h^*/m_e^*$  was approximately 2, which may promote separation of the electron–hole pairs. Therefore, the crystal and electronic structures likely contributed to the high performance of  $\text{KSb}_5\text{S}_8$  as a photocatalyst.

Finally,  $\text{KSb}_5\text{S}_8$  underwent photocorrosion due to the oxidation of metal–S bond by the photo-induced holes. Hence, preparation of a heterojunction photocatalytic system might be an effective strategy to suppress the issue of photocorrosion [30]. We also noted that the size of  $\text{KSb}_5\text{S}_8$  samples prepared in our method was of micrometer scale (Figure S7). The photocatalytic efficiency of  $\text{KSb}_5\text{S}_8$  might be improved further by generating smaller particles with a larger specific surface area to allow faster separation of photo-induced carriers and improved degradation performance. Considering the above experimental and calculated discussions, we believe that the development of a  $\text{KSb}_5\text{S}_8$ -based photocatalytic material would lead to a source of photocatalysts with layered crystal structures having excellent performance.

### 3. Experimental and Theoretical Methods

#### 3.1. Synthesis of $\text{KSb}_5\text{S}_8$

All the chemicals were purchased commercially and used without further purification. In a typical preparation, 0.8 mmol KCl, 2 mmol  $\text{Sb}_2\text{O}_3$ , and 20 mmol thiourea were mixed and grounded in an agate mortar. The mixture was then transferred to a 50 mL Teflon-lined stainless steel autoclave. The autoclave was sealed and maintained at 230 °C for 72 h. After cooling down to room temperature naturally, the final products were washed with ethanol and distilled water several times and then dried at 60 °C overnight for further characterization.

#### 3.2. Characterizations

Powder X-ray diffraction (XRD) patterns were collected on a PANalytical X'pert powder diffractometer equipped with a PIXcel detector and with  $\text{CuK}\alpha$  radiation (40 kV and 40 mA). The scanning step width was 0.01°, and the scanning rate was 0.1° s<sup>-1</sup>. Patterns were measured over the 2 $\theta$  range of 6–100°. Transmission electron microscopy (TEM), high angle annular dark field (HAADF) images, and energy dispersion spectrometry (EDS) data of  $\text{KSb}_5\text{S}_8$  were collected with a Talos F200S G2 Microscope. UV-vis diffuse reflectance spectroscopy (DRS) was performed at room temperature with a powdered  $\text{BaSO}_4$  sample as a standard on a Shimadzu UV-3150 spectrophotometer over a range of 200–900 nm.

#### 3.3. Photocatalytic Performance

The photocatalytic performance of  $\text{KSb}_5\text{S}_8$  was evaluated by degradation of methyl orange (MO). The light irradiation source was generated by an external 300 W Xe-lamp (CEL-HXF300, Beijing Aulight) with a filter ( $\lambda \geq 420$  nm) laid on the top of the reaction vessel. The temperature of the reactant solution was maintained at room temperature by providing a flow of cooling water during the photocatalytic reaction. In a typical experiment, prior to the light irradiation, the as-synthesized powder  $\text{KSb}_5\text{S}_8$  (30 mg) was dispersed in the MO solution (10 mg L<sup>-1</sup>, 100 mL), and the mixture was magnetically stirred for 60 min to achieve an adsorption–desorption equilibrium in the dark. At 30 min time intervals, 5 mL of the suspension was collected and separated by centrifugation to remove the photocatalysts. The concentration of the MO solution was monitored at 464 nm by UV-vis spectrometry.

#### 3.4. Theoretical Methods

Our calculations based on density functional theory (DFT) were performed with a plane wave basis set as implemented in the Vienna ab initio simulation package (VASP). The projector augmented wave (PAW) was used to describe the ion electron interaction. The generalized gradient approximation (GGA) was expressed by the functional of Perdew, Burke, and Ernzerhof (PBE) [31,32]. The geometry was fully relaxed until the maximum Hellmann Feynman forces were less than 0.01 eV/Å. The electronic structure, the density of states, and the partial charge density were obtained with a kinetic cut-off energy of 500 eV. K-point meshes 7 × 7 × 7 were used for electronic Brillouin zone [33]. The convergence criterion for the total energy was set to be 10<sup>-6</sup> eV.

### 4. Conclusions

In this work, we successfully synthesized sulfide  $\text{KSb}_5\text{S}_8$  through a simple solvothermal reaction, and its photocatalytic performance was examined. Structural characterization of as-synthesized  $\text{KSb}_5\text{S}_8$  was conducted by powder XRD and TEM. Additionally, UV-vis DRS results indicated that the optical band gap of  $\text{KSb}_5\text{S}_8$  was 1.62 eV, suggesting it can be used as a visible light harvesting photocatalytic material. More than 73% of an MO solution was photodegraded after visible light irradiation for 180 min, and the photocatalytic activity was approximately five and eight times greater than that of g-C<sub>3</sub>N<sub>4</sub> and commercial P25. The dynamics reaction could be described by pseudo first-order kinetics.

Our analysis of the band structure and density of states revealed that photo-induced carriers were delocalized in the layer of  $\text{KSb}_5\text{S}_8$ , and the ratio of  $m_h^*/m_e^*$  was 2. The layered crystal structure and large  $m_h^*/m_e^*$  suggest that  $\text{KSb}_5\text{S}_8$  has potential for use as a high performance photocatalyst. The findings will open up new directions for the design of a highly efficient sulfide photocatalyst with a layered crystal structure for environmental protection.

**Supplementary Materials:** The following are available online at <http://www.mdpi.com/2073-4344/9/6/529/s1>, Figure S1: UV-vis absorption of the MO solution as a function of irradiation time for  $\text{KSb}_5\text{S}_8$ ; Figure S2: The photograph of the MO solution for different irradiation time; Figure S3: Cycling performance of  $\text{KSb}_5\text{S}_8$  for the degradation of the MO solution under visible light; Figure S4: XRD patterns of  $\text{KSb}_5\text{S}_8$  after the cycling performance of photocatalytic degradation of the MO solution; Figure S5: Photodegradation of the MO solution with the additional scavenger under visible light.; Figure S6: The iso-surface of charge density with given energy window of 0.2 eV from the top and bottom of the band edge (a) VBM (b) CBM (iso-surface value 0.002); Figure S7: Optical microscopy image of  $\text{KSb}_5\text{S}_8$  from hydrothermal preparation.

**Author Contributions:** The research was completed through the cooperation of all authors. Y.L., B.Z., and D.Y. were responsible for the study of concept and design of the project. M.W., K.W. completed the experimental part, Q.W., H.Z. analyzed the data. X.Q., Y.L. and D.Y. drafted and revised the manuscript.

**Funding:** This project was supported by the Basic and Frontier Research Project of Chongqing Science and Technology Commission (Nos. cstc2018jcyjAX0827, cstc2018jcyjAX0824); The Project of Scientific and Technological Research Program of Chongqing Municipal Education Commission (Nos. KJQN201801603, KJQN201801135, KJQN201800110); The project of Science and Technology Collaborative Innovation Platform Construction of Chongqing University of Education (No. 2017XJPT01); The Cultivation for National Science Foundation of Chongqing University of Education (No. 18GZKP01); This project was funded by Children's Research Institute of National Center for Schooling Development Programme and Chongqing University of Education (No. CRIKT201909); The Scientific Research Foundation of Chongqing University of Technology (No. 0115180633).

**Conflicts of Interest:** There are no conflicts to declare.

## References

1. Chen, C.C.; Ma, W.H.; Zhao, J.C. Semiconductor-mediated photo-degradation of pollutants under visible light irradiation. *Chem. Soc. Rev.* **2010**, *39*, 4206–4219. [[CrossRef](#)] [[PubMed](#)]
2. Li, H.H.; Gao, Y.J.; Gao, D.Q.; Wang, Y.H. Effect of Oxide Defect on Photocatalytic Properties of  $\text{MSnO}_3$  (M = Ca, Sr and Ba) Photo-catalysts. *Appl. Catal. B Environ.* **2019**, *243*, 428–437. [[CrossRef](#)]
3. Kim, D.H.; Yeo, H.C.; Shin, D.B.; Choi, H.; Kim, S.; Park, N.; Han, S.S. Dissimilar Anisotropy of Electron Versus Hole Bulk Transport in Anatase  $\text{TiO}_2$ : Implications for Photo-catalysis. *Phys. Rev. B* **2017**, *95*, 045209–045214. [[CrossRef](#)]
4. Hussain, H.; Tocci, G.; Woolcot, T.; Torrelles, X.; Pang, C.L.; Humphrey, D.S.; Yim, C.M.; Grinter, D.C.; Cabailh, G.; Bikondoa, O.; et al. Structure of a Model  $\text{TiO}_2$  Photocatalytic Interface. *Nat. Mater.* **2017**, *16*, 461–466. [[CrossRef](#)] [[PubMed](#)]
5. Stecher, T.; Reuter, K.; Oberhofer, H. First Principles Free Energy Barriers for Photo-electrochemical Surface Reactions: Proton Abstraction at  $\text{TiO}_2(110)$ . *Phys. Rev. Lett.* **2016**, *117*, 276001–276007. [[CrossRef](#)] [[PubMed](#)]
6. Zhou, M.L.; Jiang, X.; Jiang, X.X.; Xiao, K.; Guo, Y.W.; Huang, H.W.; Lin, Z.S.; Yao, J.Y.; Tung, C.H.; Wu, L.Z.; et al.  $\text{Wu, BaAu}_2\text{S}_2$ : A Au-Based Intrinsic Photo-catalyst for High Performance Visible Light Photo-catalysis. *Inorg. Chem.* **2017**, *56*, 5173–5181. [[CrossRef](#)] [[PubMed](#)]
7. Yaghoubi, H.; Li, Z.; Chen, Y.; Ngo, H.T.; Bhethanabotla, V.R.; Joseph, H.; Ma, S.Q.; Schlaf, R.; Takshi, A. Toward a Visible Light-Driven Photo-catalyst: The Effect of Midgap-States-Induced Energy Gap of Undoped  $\text{TiO}_2$  Nanoparticles. *ACS Catal.* **2015**, *5*, 327–335. [[CrossRef](#)]
8. Wen, B.; Yin, W.J.; Selloni, A.; Liu, L.M. Defects, Adsorbates and Photo-activity of Rutile  $\text{TiO}_2(110)$ : Insight by First Principles Calculations. *J. Phys. Chem. Lett.* **2018**, *9*, 5281–5287. [[CrossRef](#)]
9. Liu, L.C.; Ji, Z.Y.; Zou, W.X.; Gu, X.R.; Deng, Y.; Gao, F.; Tang, C.J.; Dong, L. In Situ Loading Transition Metal Oxide Clusters on  $\text{TiO}_2$  Nano-sheets As Co-catalysts for Exceptional High Photo-activity. *ACS Catal.* **2013**, *3*, 2052–2061. [[CrossRef](#)]
10. David, S.; Mahadik, M.A.; Chung, H.S.; Ryu, J.H.; Jang, J.S. Facile Hydrothermally Synthesized a Novel CdS Nanoflower/Rutile- $\text{TiO}_2$  Nanorod Heterojunction Photoanode Used for Photo-electro-catalytic Hydrogen Generation. *ACS Sustain. Chem. Eng.* **2017**, *5*, 7537–7548. [[CrossRef](#)]

11. Yan, T.J.; Li, L.P.; Li, G.S.; Wang, Y.J.; Hu, W.B.; Guan, X.F. Porous SnIn<sub>4</sub>S<sub>8</sub> Microspheres in a New Polymorph that Promotes Dyes Degradation under Visible Light Irradiation. *J. Hazard. Mater.* **2011**, *186*, 272–279. [[CrossRef](#)] [[PubMed](#)]
12. Yang, J.; Fu, H.; Yang, D.F.; Gao, W.L.; Cong, R.H.; Yang, T. ZnGa<sub>2-x</sub>In<sub>x</sub>S<sub>4</sub> (0 < x < 0.4) and Zn<sub>1-2y</sub>(CuGa)<sub>y</sub>Ga<sub>1.7</sub>In<sub>0.3</sub>S<sub>4</sub> (0.1 < y < 0.2): Optimize Visible Light Photocatalytic H<sub>2</sub> Evolution by Fine Modulation of Band Structures. *Inorg. Chem.* **2015**, *54*, 2467–2473. [[PubMed](#)]
13. Zhao, Q.Y.; Guo, Y.H.; Zhou, Y.X.; Yao, Z.H.; Ren, Z.Y.; Bai, J.T.; Xu, X.L. Band Alignments and Hetero-structures of Monolayer Transition Metal Trichalcogenides MX<sub>3</sub> (M = Zr, Hf; X = S, Se) and Di-chalcogenides MX<sub>2</sub> (M = Tc, Re; X = S, Se) for Solar Applications. *Nanoscale* **2018**, *10*, 3547–3555. [[CrossRef](#)] [[PubMed](#)]
14. Kuhar, K.; Crovetto, A.; Pandey, M.; Thygesen, K.S.; Seger, B.; Vesborg, P.C.K.; Hansen, O.; Chorkendorff, I.K.; Jacobsen, W. Sulfide Perovskites for Solar Energy Conversion Applications: Computational Screening and Synthesis of the Selected Compound LaYS<sub>3</sub>. *Energy Environ. Sci.* **2017**, *10*, 2579–2593. [[CrossRef](#)]
15. Mir, S.H.; Chakraborty, S.; Warna, J.; Narayan, S.; Jha, P.C.; Jha, P.K.; Ahuja, R. A Comparative Study of Hydrogen Evolution Reaction on Pseudo Monolayer WS<sub>2</sub> and PtS<sub>2</sub>: Insights Based on the Density Functional Theory. *Catal. Sci. Technol.* **2017**, *7*, 687–692. [[CrossRef](#)]
16. Zhu, X.X.; Luo, X.K.; Yuan, H.K.; Chen, H.; Tian, C.L. Band Gap Engineering of SnS<sub>2</sub> Nanosheets by Anion-Anion Co-doping for Visible Light Photo-catalysis. *RSC Adv.* **2018**, *8*, 3304–3313. [[CrossRef](#)]
17. Zhang, X.; Zhao, X.D.; Wu, D.H.; Jing, Y.; Zhou, Z. MnPSe<sub>3</sub> Monolayer: A Promising 2D Visible Light Photohydrolytic Catalyst with High Carrier Mobility. *Adv. Sci.* **2016**, *3*, 1600062–1600066. [[CrossRef](#)] [[PubMed](#)]
18. Campbell, Q.; Fisher, D.; Dabo, I. Voltage-dependent Reconstruction of Layered Bi<sub>2</sub>WO<sub>6</sub> and Bi<sub>2</sub>MoO<sub>6</sub> Photocatalysts and Its Influence on Charge Separation for Water Splitting. *Phys. Rev. Mater.* **2019**, *3*, 015404. [[CrossRef](#)]
19. Xiong, T.; Cen, W.L.; Zhang, Y.X.; Dong, F. Bridging the g-C<sub>3</sub>N<sub>4</sub> Interlayers for Enhanced Photo-catalysis. *ACS Catal.* **2016**, *6*, 2462–2472. [[CrossRef](#)]
20. Li, Z.J.; Qu, Y.; Hu, K.; Humayun, M.; Chen, S.Y.; Jing, L.Q. Improved Photo-electrocatalytic Activities of BiOCl with High Stability for Water Oxidation and MO degradation by Coupling RGO and Modifying Phosphate Groups to Prolong Carrier Lifetime. *Appl. Catal. B Environ.* **2017**, *203*, 355–362. [[CrossRef](#)]
21. Wachter, J.B.; Chrissafis, K.; Petkov, V.; Malliakas, C.D.; Bilc, D.; Kyratsi, T.; Paraskevopoulos, K.M.; Mahanti, S.D.; Torbrugge, T.; Eckert, H.; et al. Local Structure and Influence of Bonding on the Phase-Change Behavior of the Chalcogenide Compounds K<sub>1-x</sub>Rb<sub>x</sub>Sb<sub>5</sub>S<sub>8</sub>. *J. Solid State Chem.* **2007**, *180*, 420–431. [[CrossRef](#)]
22. Kyratsi, T.; Chrissafis, K.; Wachter, J.; Paraskevopoulos, K.M.; Kanatzidis, M.G. KSb<sub>5</sub>S<sub>8</sub>: A Wide Bandgap Phase-Change Material for Ultra High Density Rewritable Information Storage. *Adv. Mater.* **2003**, *15*, 1428–1430. [[CrossRef](#)]
23. Berlepsch, P.; Miletich, R.; Armbruster, T. The Crystal Structures of Synthetic KSb<sub>5</sub>S<sub>8</sub> and (Tl<sub>0.598</sub>, K<sub>0.402</sub>) Sb<sub>5</sub>S<sub>8</sub> and their relation to parapirotite (TlSb<sub>5</sub>S<sub>8</sub>). *Z. Krist.* **1999**, *214*, 57–63. [[CrossRef](#)]
24. Liu, J.; Fan, X.Y.; Zhu, Y.Q.; Zhao, J.; Jiang, F.X.; Chen, S.; Sun, H.; Xu, J.K.; Deng, W.Y.; Wang, C.Y. Efficient Photo-dechlorination of Chlorophenols on Polarized MZnB<sub>5</sub>O<sub>10</sub> (M = Na and K) Nonlinear Optical Materials. *Appl. Catal. B Environ.* **2016**, *181*, 436–444. [[CrossRef](#)]
25. Zhuang, H.L.; Hennig, R.G. Theoretical Perspective of Photocatalytic Properties of Single Layer SnS<sub>2</sub>. *Phys. Rev. B* **2013**, *88*, 115314–115318. [[CrossRef](#)]
26. Fan, X.Y.; Wu, Z.P.; Wang, L.C.; Wang, C.Y. Exploring the Origin of High Dechlorination Activity in Polar Materials M<sub>2</sub>B<sub>5</sub>O<sub>9</sub>Cl (M = Ca, Sr, Ba and Pb) with Built-in Electric Field. *Chem. Mater.* **2017**, *29*, 639–647. [[CrossRef](#)]
27. Li, B.S.; Lai, C.; Zeng, G.M.; Qin, L.; Yi, H.; Huang, D.L.; Zhou, C.Y.; Liu, X.G.; Cheng, M.; Xu, P.; et al. Facile Hydrothermal Synthesis of Z-scheme Bi<sub>2</sub>Fe<sub>4</sub>O<sub>9</sub>/Bi<sub>2</sub>WO<sub>6</sub> Heterojunction Photo-catalyst with Enhanced Visible Light Photocatalytic Activity. *ACS Appl. Mater. Interfaces* **2018**, *10*, 18824–18836. [[CrossRef](#)]
28. Harb, M.; Cavallo, L. Suitable Fundamental Properties of Ta<sub>0.75</sub>V<sub>0.25</sub>ON Material for Visible Light Driven Photo-catalysis: A DFT Study. *ACS Omega* **2016**, *1*, 1041–1048. [[CrossRef](#)]
29. Ma, Z.J.; Yi, Z.G.; Sun, J.; Wu, K.C. Electronic and Photocatalytic Properties of Ag<sub>3</sub>PC<sub>4</sub> (C = O, S, Se): A Systemic Hybrid DFT Study. *J. Phys. Chem. C* **2012**, *116*, 25074–25080. [[CrossRef](#)]

30. Yan, T.J.; Tian, J.; Guan, W.F.; Qiao, Z.; Li, W.J.; You, J.M.; Huang, B.B. Ultra-low Loading of  $\text{Ag}_3\text{PO}_4$  on Hierarchical  $\text{In}_2\text{S}_3$  Microspheres to Improve the Photo-catalytic Performance: The Cocatalytic Effect of Ag and  $\text{Ag}_3\text{PO}_4$ . *Appl. Catal. B Environ.* **2017**, *202*, 84–94. [[CrossRef](#)]
31. Blochl, P.E. Projector Augmented Wave Method. *Phys. Rev. B* **1994**, *50*, 17953–17979. [[CrossRef](#)]
32. Perdew, J.P.; Burke, K.; Ernzerhof, M. Generalized Gradient Approximation Made Simple. *Phys. Rev. Lett.* **1996**, *77*, 3865–3868. [[CrossRef](#)] [[PubMed](#)]
33. Monkhorst, H.J.; Pack, J.D. Special Points for Brillouin Zone Integrations. *Phys. Rev. B* **1976**, *13*, 5188–5192. [[CrossRef](#)]



© 2019 by the authors. Licensee MDPI, Basel, Switzerland. This article is an open access article distributed under the terms and conditions of the Creative Commons Attribution (CC BY) license (<http://creativecommons.org/licenses/by/4.0/>).